Journal of Alloys and Compounds 653 (2015) 358–362

Contents lists available at ScienceDirect

Journal of Alloys and Compounds

journal homepage: http://www.elsevier.com/locate/jalcom

The role of defects on the structural and magnetic properties of Nb_2O_5

Leonilson K.S. Herval [a], Driele von Dreifus [b], Adriano C. Rabelo [b], Ariano D. Rodrigues [a], Ernesto C. Pereira [b], Yara G. Gobato [a], Adilson J.A. de Oliveira [a], Marcio P.F. de Godoy [a, *]

[a] Departamento de Física, Universidade Federal de São Carlos (UFSCAR) 13560-905, São Carlos, SP, Brazil
[b] Departamento de Química, Universidade Federal de São Carlos (UFSCAR) 13560-905, São Carlos, SP, Brazil

ARTICLE INFO

Article history:
Received 31 July 2015
Accepted 1 September 2015
Available online 8 September 2015

Keywords:
Oxide materials
Sol–gel processes
Magnetization
Optical spectroscopy
Raman
Dilute magnetic semiconductors

ABSTRACT

Defects play a fundamental issue on physical properties of wide bandgap materials. We present here the effect of preparation and annealing conditions on the properties of Nb_2O_5 synthesized by Pechini method. Structural characterization, Raman spectroscopy and magnetic measurements show significant experimental fingerprints related to the presence of oxygen defects in the system. The increase of oxygen vacancies causes an irreversible phase transition from pseudohexagonal (TT-phase) to orthorhombic phase (T-phase). The critical temperature range around 400 °C during thermal annealing is derived by in-situ Raman measurements applying the theory of phonon anharmonicity. We observed that the values of Nb_2O_5 Curie constants as $(4.37 \pm 0.06)10^{-4}$ emu K/mol and $(20.50 \pm 0.08)10^{-4}$ emu K/mol for TT- and T-phases respectively. The oxygen vacancies are the responsible for 10^{21}–10^{22} effective magnetic moments per mol related to paramagnetic behavior.

1. Introduction

In the last years, the synthesis of oxide nanomaterials such as TiO_2, MnO_2, ZnO, VO_x and Nb_2O_5 have attracted attention due their physical and chemical properties as wide bandgap, piezoelectricity, electrochromism, that can be used in chemical sensors, optical filters, solar cells, among others. An interesting feature about these properties is the influence of oxygen-related defects such as vacancies (V_O) in the optical [1], electrical [2] and magnetic [3–6] characteristics of oxides which emerges as an active research field due to their importance in both scientific and application possibilities. It is a common sense that the structure and morphology of oxides depend drastically on the synthesis method and experimental variables. Different preparation conditions, even though using the same methodology, can produce samples with different structural and magnetic properties. Therefore, the control of growth parameters is an important issue in the area of materials engineering.

Due to its fairly unreactive, colorless nature and large number of industrial (such as electronic components as capacitor and optical glasses [7,8]) the most common niobium compound, Niobium Pentoxide (Niobic Anhydride, Nb_2O_5), is particularly interesting [9,10]. Consequently the comprehension of synthesis method and the employed post-thermal conditions are essential to control the influence of defects and their dependent physical properties. In the literature, there are many synthesis pathways described to prepare this material, such as hydro post-thermal and mechanochemical procedures [11], and different sol–gel methods [12,13]. One of later, the Pechini method has been used to produce high homogeneous samples at low cost and simplicity.

Considering the exposed above, our work explores the effects of intrinsic defect formation during the preparation of Nb_2O_5 at different calcination temperatures and correlate them with extrinsic defects induced by post-thermal annealing under an inert atmosphere for the synthesized pseudohexagonal (TT-phase) Nb_2O_5. Structural analysis correlated to Raman spectroscopy shows that the transition from pseudohexagonal to orthorhombic (T-phase) is associated to the introduction of oxygen vacancy defects in both processes. Furthermore a strong increase of magnetic moments associated to of these defects was observed in T-phase.

2. Experiment

Nb_2O_5 powders were prepared by Pechini method and exhibits two crystalline phases. The employed method is schematized in Fig. 1. The process starts by heating ethylene glycol at 60 °C and then adding citric acid. After that the niobium precursor, the

* Corresponding author.
E-mail address: mgodoy@ufscar.br (M.P.F. de Godoy).

http://dx.doi.org/10.1016/j.jallcom.2015.09.019
0925-8388/

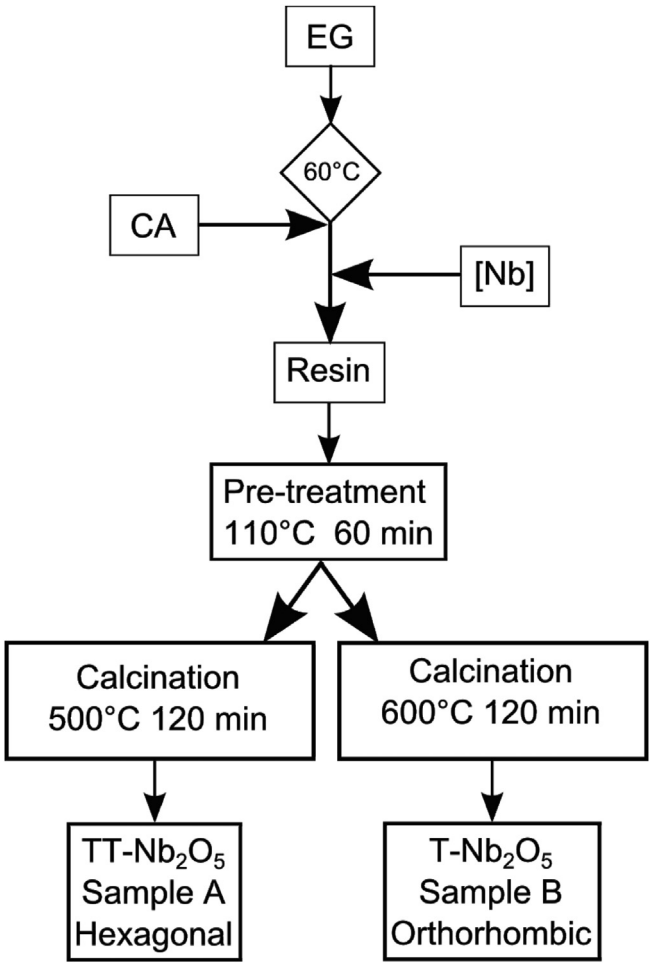

Fig. 1. Schematic representation for Nb_2O_5 preparation.

complex $NH_4H_2[NbO(C_2O_4)_3]\cdot 3H_2O$ is added to the mixture until complete dissolution. In this work the employed solution has a proportion 1:10:40 between niobium precursor, citric acid and ethylene glycol respectively. The temperature of calcination is an important parameter on crystallization process and structural properties of Nb_2O_5 [14]. As a consequence, two different samples were prepared: i) one calcined at 500 °C and ii) other calcined at 600 °C.

X-Ray diffractometry (XRD) and Raman spectroscopy measurements were carried out to analyze the crystalline structure of the samples. XRD were measured with a diffractometer Rigaku 12500PC operating with Cu–K_α as radiation line ($\lambda = 1.5478$ Å). The Raman spectra were collected by a Jobin-Yvon triple grating spectrometer with microscope facilities, using as excitation source the line with wavelength 514 nm of an Ar^+/Kr^+. The influence of defects on the magnetic behavior was analyzed by magnetization measurements as a function of applied magnetic field up to 70 kOe and in the range of temperature of 1.8 K–300 K, performed using a SQUID-VSM magnetometer (MPMS®3-Quantum Design).

3. Results and discussion

XRD data of samples are displayed in Fig. 2a and b and compared with the diffraction patterns for the pseudohexagonal phase TT-Nb_2O_5 (JCPDS 7-61) and orthorhombic phase T-Nb_2O_5 (JCPDS 30-873) (Fig. 2c and d). We observe from the figure that the calcination temperature is an important parameter during the Nb_2O_5 synthesis.

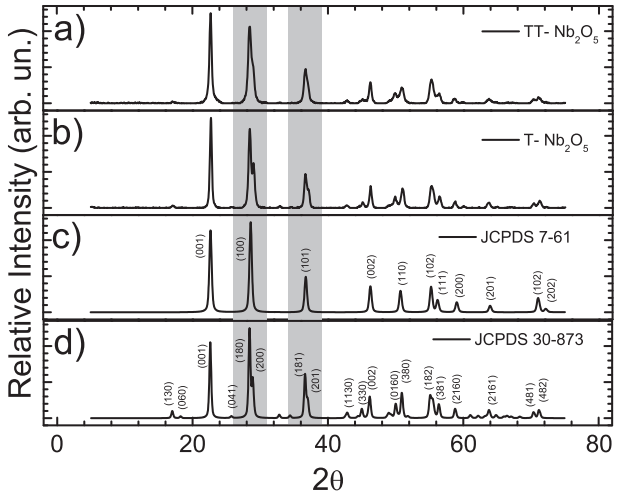

Fig. 2. X-ray diffraction of Nb_2O_5: a) TT-phase; b) T-phase and the patterns c) JCPDS 7-61 and d) JCPDS 30-873.

The main differences between the patterns can be noticed in the range between 25° and 40°. The pseudohexagonal phase presents only one peak in each hachured area, related to the diffraction of (100) and (101) planes while for the orthorhombic structure these peaks split which are attributed the (180)–(200) and (181)–(201) planes [15]. Based in these results we conclude that the sample calcined at 500 °C presents predominantly the pseudohexagonal (TT) phase, while the sample calcined at 600 °C has solely orthorhombic (T) phase. However the transition temperature is described to depend on different factors, such as the starting material, level of impurity and heating schedule [16]. The major difference between these two phases is attributed to the replacement of oxygen atoms in TT-phase by impurities or vacancies [17].

The crystallite size (D) in hkl direction of the samples were estimated using the Scherrer equation [18] (Eq. (1)) for the highest intensity peak.

$$D = \frac{K\lambda}{\beta cos\theta}, \quad (1)$$

where λ is the wavelength for the Cu–K_α radiation (1.5406 Å), K is an empirical constant (0.9) and β is the full width at half maximum (FWHM) in radians. The obtained values summarized in Table 1 indicate a moderate increase of D value for the orthorrombic sample.

Raman spectroscopy has been widely employed as a powerful tool to investigate structural, chemical and periodical effects in poly- and monocrystalline materials [19,20]. In particular, the investigation of intensity and position of peaks related to some vibrational modes from Nb_2O_5 allow the analysis of bounds between niobium and oxygen in each phase [21]. Fig. 3 shows the Raman spectra related to Nb_2O_5 samples. We observe three broad bands related to Nb_2O_5 at 690 cm^{-1}, 315 cm^{-1} and 227 cm^{-1}, labeled as Peak 1, 2 and 3 respectively. The Peak 1, at higher

Table 1
Crystallite size (D) in (100) direction and the relative intensity ΔI related to Raman peaks associated to Nb–O–Nb angle deformations.

Nb_2O_5	D (Å)	ΔI
TT-phase	215	0.073
T-phase	246	0.116
Annealed sample	345	0.135

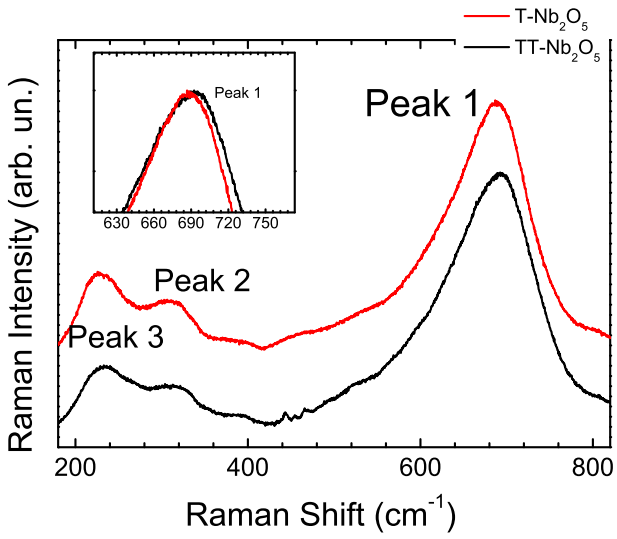

Fig. 3. Raman spectra of Nb_2O_5. The Peak 1 corresponds to Nb–O–Nb bridging bond and Peaks 2 and 3 to Nb–O–Nb angle deformations. The inset shows the different energies of the Peak 1 for TT and T-phases.

frequency, is related to Nb–O–Nb bridging bond of distorted NbO_6 [21]. Usually this peak is important to identify the Nb_2O_5 structural phases [22]. It is possible to notice in the inset of Fig. 3 a redshift about 3.4 cm^{-1} from the TT-Nb_2O_5 to T-Nb_2O_5. Generally the redshift occurs when the lattice parameter increases [23] like in thermal expansion or structural phase transitions.

Angle deformations related to Nb–O–Nb bounds are associated to the low frequencies peaks 2 and 3 (315 cm^{-1} and 227 cm^{-1} respectively). From the spectra of samples TT-Nb_2O_5 and T-Nb_2O_5 it is noticeable a slight difference in the relative intensity of the peaks 2 and 3, which are associated to a rearrangement in the angle deformation [21]. As an evaluation of these structural distinctions we propose to calculate the relative difference intensities ΔI between the angle deformations peaks (I_2 and I_3) normalized to bridging bond peak (I_1):

$$\Delta I = \frac{I_3 - I_2}{I_1}. \quad (2)$$

For pseudohexagonal phase we obtained $\Delta I_{TT} = 0.073$, while for orthorhombic phase $\Delta I_T = 0.116$, which corresponds to an increase of about 60%. As a consequence ΔI can be interpreted as an empirical indicative of crystalline phase.

In order to investigate the nature of structural phases we carried out Raman spectroscopy measurements during a thermal annealing under N_2 flux atmosphere for the TT-phase sample. The *in-situ* Raman spectra were collected up to 750 °C as depicted in Fig. 4a. The spectra show the changes between ΔI which are correlated to modifications in the angle deformations of Nb–O–Nb bounds. During heating treatment under N_2 flux, a process of reduction causes a rearrangement of Nb atomic positions, leading to a structural modification to the orthorhombic phase. There was an increase in the parameter ΔI after cooldown (ΔI = 0.135) as well as for crystallite size measured by posterior XRD as indicated in Table 1.

During a phase transition the lattice parameters increases from TT-Nb_2O_5 (a = b = 3.607 Å) to T-Nb_2O_5 (a = 6.175 Å and b = 28.25 Å). Fig. 4b shows the pseudohexagonal unit cell which contains half of the equivalent formula ($NbO_{2.5}$), with constitutional defects of one oxygen atom per unit cell [21]. A structure chain Nb–O–Nb–O is observed along the c-axis and each Nb atom is surrounded by four, five or six oxygen atoms in the ab-plane. The polyhedral are distorted by oxygen deficiency. Moreover in the orthorhombic phase there is an absence of oxygen atoms resulting in the modification of Nb neighborhood. In this case each Nb atom is surrounding by six or seven oxygen atoms, forming a distorted octahedral or pentagonal bipyramids. The ab-plane (Fig. 4c) are connected by edge- or corner-sharing and by corner-shared along the c-axis [21,24]. Considering data described in the literature and the Raman results obtained in this work, we interpret the increase of ΔI parameter as a result of oxygen migration from their original sites which is responsible for the structural changes. Thus the ΔI parameter can be used as a signature of oxygen defects which causes changes in the angles of Nb–O–Nb bonds.

Besides analyzing the variation in ΔI parameter induced by the thermal treatment, which enabled the phase transition determination, we have also studied the changes of the energies of peaks 2 and 3 as the annealing temperature increased. To determine the spectral position of the peaks with accurate precision, we fitted the lowest energy range of all spectra shown in Fig. 4a using two peaks. One example of this spectral decomposition can be seen in the inset of Fig. 5. The figure also depicts the central positions of peaks 2 and 3 as a function of the sample temperature. The positions correspond to the best fit achieved for all the spectra taken *in situ*.

It can be noticed that the Peak 2 has a blueshift as the temperature increases. This variation is attributed to the decay of a zone-center optical phonon via anharmonicity to acoustic phonons presenting momenta with equal magnitude and opposite direction [25]. The relation between the central position of the peak and the temperature is given by a monotonic function which depends of anharmonic coefficients, associated to the properties of the decay process. The red (in web version) line in Fig. 5 presents the peak position as a function of temperature Ω(T) calculated by the theory presented in Ref. [25].

$$\Omega(T) = \omega_0 + C\left[1 + \frac{2}{e^{\frac{\hbar\omega_0}{2k_BT}} - 1}\right] + D\left[1 + \frac{3}{e^{\frac{\hbar\omega_0}{3k_BT}} - 1} + \frac{3}{\left(e^{\frac{\hbar\omega_0}{3k_BT}} - 1\right)^2}\right] \quad (3)$$

where ω_0,C and D are anharmonic coefficients based on three and four phonon processes, and k_B and ħ are the Boltzmann and Planck constants.

By adjusting the anharmonic coefficients we could find a theoretical dependence between peak energies and temperature that presents a good agreement with the experimental data. For peak 2 (Fig. 5a) we obtained ω_0 = 228 cm^{-1}, C = 0.45 cm^{-1} and D = 0.05 cm^{-1}. Peak 1 (not shown here) follows the theory of phonon anharmonicity with ω_0 = 708 cm^{-1}, C = −20 cm^{-1} and D = 1.26 cm^{-1}. In Fig. 5b we can notice that the Peak 3 does not present any similar behavior. When the temperature is increased up to 400 °C its central position progressively goes to lower energies, but adopts an upward trend when the temperature is further increased. Then, the relation between the energy of the Peak 3 and the temperature does not describe a monotonic behavior in the whole temperature range and, consequently, cannot be related to a normal anharmonic effect of an optical phonon. In contrast, the inversion of the tendency indicates that this vibrational mode present a different nature for temperatures higher than 400 °C due to a rearrangement in Nb–O–Nb bonds. During the applied post-thermal treatment, this must be the temperature value for which the oxygen defects give rise significantly in the material.

Oxygen vacancies were reported as an important issue for magnetic properties [3–6]. The Fig. 6 shows the magnetic

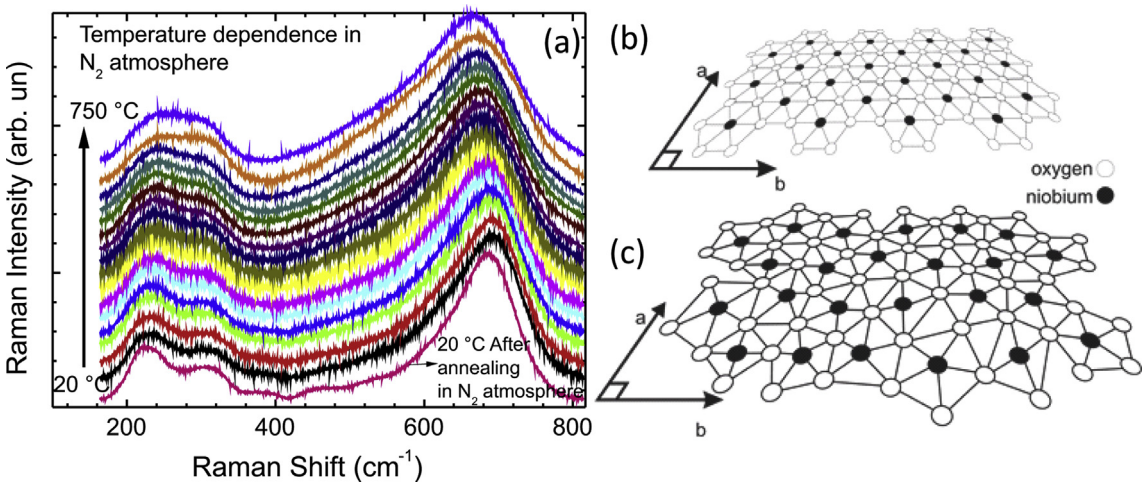

Fig. 4. (a) Raman spectra taken *in situ* during annealing in N_2 atmosphere; (b) and (c) structural schemes of TT-Nb_2O_5 and T-Nb_2O_5, respectively.

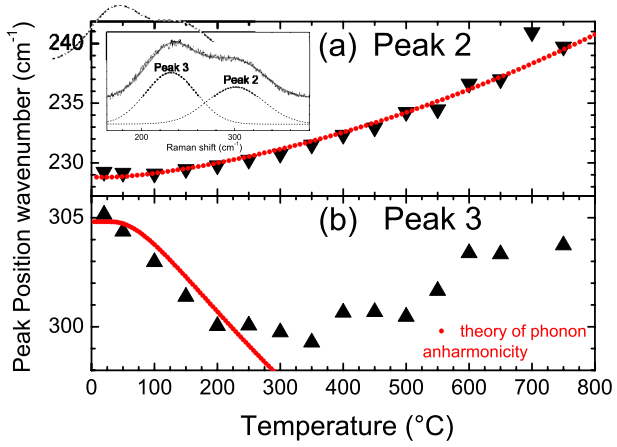

Fig. 5. Central positions of Peaks 2 and 3 for TT-phase as a function of temperature and the expected behavior by theory of phonon anharmonicity. The inset shows the fitting procedure where the solid black line is the experimental spectrum and the gray line is its best fit.

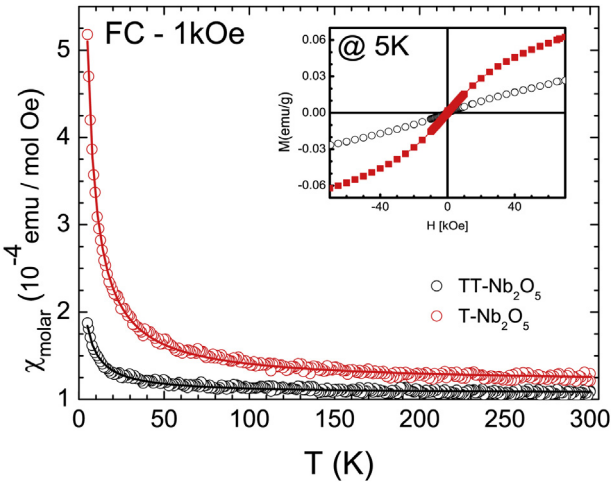

Fig. 6. Susceptibility versus temperature for TT and T-phases of Nb_2O_5. The best fit data to Curie law is shown as solid lines.

susceptibility ($\chi = M/H$) as a function of the temperature, whose data were obtained in order to better understand the magnetic behavior of these samples. In the inset we can observe the magnetization as a function of applied magnetic field without any evidence of coercive field and remanent magnetization.

The results show a paramagnetic behavior that can be describe using the paramagnetic Curie equation [19].

$$\chi = \frac{C_0}{T} + \chi_0, \tag{4}$$

where C_0 is the Curie constant and χ_0 was added to represent the temperature independent paramagnetism. The Curie constant is also defined as

$$C_0 = \frac{\mu_B^2}{3k_B} Ng^2 J(J+1) = \frac{\mu_B^2}{3k_b} p^2 N, \tag{5}$$

where μ_B is the Bohr magneton, k_B is the Boltzmann constant and p^2N is the effective moments which contribute to the paramagnetic behavior. The fitting results are show in Table 2.

We report that the Curie constants for TT- and T-phases of Nb_2O_5 present a substantial increment (~370%) due to the phase transition. This effect is associated to the increase of oxygen vacancies, that are the responsible for increasing the magnetic susceptibility in T-phase. The number of effective moments in the range between 10^{21}–10^{22} per mol avoids the short-range magnetic interactions and the Nb_2O_5 is then considered a Curie paramagnet. In fact, these results show that the presence of oxygen vacancies, as shown from Raman measurements, lead to the formation of magnetic moments.

4. Conclusions

Using Pechini method we have produced niobium pentoxide (Nb_2O_5) in two structural phases: pseudohexagonal (TT-phase) and orthorhombic (T-phase) strongly dependent on calcination temperature. A thermal treatment in TT-phase Nb_2O_5 under N_2 atmosphere up to 750 °C caused an irreversible structural transition to T-phase. The features in Raman spectra (Peaks at 315 cm^{-1} and 227 cm^{-1}) obtained in-situ during annealing provided two signatures related to angle deformations peaks at 315 cm^{-1} and 227 cm^{-1}: i) the empirical parameter ΔI of their relative intensities and ii) the disagreement with the phonon anharmonicity theory due to a rearrangement in Nb—O—Nb bonds above 400 °C.

Table 2
Curie–Weiss fitting results: Curie constant C_0, temperature independent paramagnetism χ_0 and the effective number of moments Np^2.

FC 1 kOe	C_0 (10^{-4} emu K/mol)	χ_0 (10^{-4} emu/mol Oe)	Np^2 (10^{21} effective moments per mol)
TT − Nb_2O_5	4.37 ± 0.06	1.08 ± 0.01	2.1 ± 0.1
T − Nb_2O_5	20.50 ± 0.08	1.202 ± 0.002	9.9 ± 0.1

Correlations between the data show that the main differences between these phases are due to the introduction of oxygen defects during higher calcination temperatures as well as in post-thermal treatment. The oxygen vacancies are the responsible for the formation of magnetic moments and the observed paramagnetic behavior. The enhancement of effective magnetic moments in one order of magnitude induces the increase of Curie constant up to 370% and justify their influence on the paramagnetic behavior of Nb_2O_5.

Acknowledgments

This work was supported partially from Brazilians agencies FAPESP (grants 2013/17657-2 and 2012/24025-0), CNPq (grant 474411/2013-3) and CAPES.

References

[1] P.A. Rodnyi, I.V. Khodyuk, Opt. Spectrosc. 111 (2011) 776.
[2] I. Balint, K.-I. Aika, Appl. Surf. Sci. 173 (2001) 296.
[3] M.P.F. de Godoy, A. Mesquita, W. Avansi, P.P. Neves, V.A. Chitta, W.B. Ferraz, M.A. Boselli, A.C.S. Sabioni, H.B. de Carvalho, J. Alloys Compd. 555 (2013) 315.
[4] V. Fernandes, R.J.O. Mossanek, P. Schio, J.J. Klein, A.J.A. de Oliveira, W.A. Ortiz, N. Mattoso, J. Varalda, W.H. Schreiner, M. Abbate, D.H. Mosca, Phys. Rev. B 80 (2009) 035202.
[5] D. Von Dreifus, A.J.A. de Oliveira, A.V. do Rosario, E.C. Pereira, J. Supercond. Nov. Magn. 26 (2013) 2319.
[6] J.M.D. Coey, Solid State Sci. 7 (2005) 660.
[7] A. I. d. Sá, C.M. Rangel, P. Skeldon, G.E. Thompson, Port. Electrochimica Acta 24 (2006) 305.
[8] F. Lai, L. Lin, Z. Huang, R. Gai, Y. Qu, Appl. Surf. Sci. 253 (2006) 1801.
[9] H. Luo, M. Wei, K. Wei, J. Nanomater. 2009 (2009) 4.
[10] M.P.F. Graça, A. Meireles, C. Nico, M.A. Valente, J. Alloys Compd. 553 (2013) 177.
[11] M. Ristić, S. Popović, S. Musić, Mater. Lett. 58 (2004) 2658.
[12] K. Sayama, H. Sugihara, H. Arakawa, Chem. Mater. 10 (1998) 3825.
[13] M.A. Aegerter, M. Schmitt, Y. Guo, Int. J. Photoenergy 4 (2002).
[14] M.A. Aegerter, Sol. Energy Mater. Sol. Cells 68 (2001) 401.
[15] A. Rosario, E. Pereira, J. Solid State Electrochem. 9 (2005) 665.
[16] E.I. Ko, J.G. Weissman, Catal. Today 8 (1990) 27.
[17] I. Nowak, M. Ziolek, Chem. Rev. 99 (1999) 3603.
[18] A.L. Patterson, Phys. Rev. 56 (1939) 978.
[19] H.B. de Carvalho, M.P.F. de Godoy, R.W.D. Paes, M. Mir, A. Ortiz de Zevallos, F. Iikawa, M.J.S.P. Brasil, V.A. Chitta, W.B. Ferraz, M.A. Boselli, A.C.S. Sabioni, J. Appl. Phys. 108 (2010) 033914.
[20] A.D. Rodrigues, M.P.F. de Godoy, C. Mietze, D.J. As, Solid State Commun. 186 (2014) 18.
[21] T. Ikeya, M. Senna, J. Non Cryst. Solids 105 (1988) 243.
[22] J.-M. Jehng, I.E. Wachs, Catal. Today 8 (1990) 37.
[23] O.A. Yassin, S.N. Alamri, A.A. Joraid, J. Phys. D Appl. Phys. 46 (2013) 235301.
[24] E. Tsang, X. Zhou, L. Ye, S.C. Edman Tsang, Nano Rev. 3 (2012) 17631.
[25] M. Balkanski, R.F. Wallis, E. Haro, Phys. Rev. B 28 (1983) 1928.